Ergoregion instability of ultracompact astrophysical objects

Vitor Cardoso[*]
Department of Physics and Astronomy, The University of Mississippi, University, Mississippi 38677-1848, USA

Paolo Pani[+]
Dipartimento di Fisica, Università di Cagliari, Cittadella Universitaria 09042 Monserrato, Italy, and Department of Physics and Astronomy, The University of Mississippi, University, Mississippi 38677-1848, USA

Mariano Cadoni[‡]
Dipartimento di Fisica, Università di Cagliari, and INFN sezione di Cagliari, Cittadella Universitaria 09042 Monserrato, Italy

Marco Cavaglià[§]
Department of Physics and Astronomy, The University of Mississippi, University, Mississippi 38677-1848, USA
(Received 15 September 2007; published 26 June 2008)

Most of the properties of black holes can be mimicked by horizonless compact objects such as gravastars and boson stars. We show that these ultracompact objects develop a strong ergoregion instability when rapidly spinning. Instability time scales can be of the order of 0.1 seconds to 1 week for objects with mass $M = 1 - 10^6 M_\odot$ and angular momentum $J > 0.4M^2$. This provides a strong indication that ultracompact objects with large rotation are black holes. Explosive events due to ergoregion instability have a well-defined gravitational-wave signature. These events could be detected by next-generation gravitational-wave detectors such as Advanced LIGO or LISA.

DOI: 10.1103/PhysRevD.77.124044 PACS numbers: 04.40.Dg, 04.25.Nx, 04.30.Nk, 95.85.Sz

I. INTRODUCTION

Black holes (BHs) in Einstein-Maxwell theory are characterized by three parameters [1]: Mass M, electric charge Q, and angular momentum $J \equiv aM \leq M^2$. BHs are thought to be abundant objects in the Universe [2]. Their mass is estimated to vary between $3M_\odot$ and $10^{9.5}M_\odot$ or higher. They are likely to be electrically neutral because of the effect of surrounding plasma [3] and their angular momentum is expected to be close to the extremal limit because of accretion and merger events [4,5]. An example of an astrophysical BH is the compact primary of the binary x-ray source GRS 1915 + 105, which recent observations identify as a rapidly rotating object of spin $a \gtrsim 0.98M$ [6]. Many of the supermassive BHs which are thought to power quasars seem to be rotating near the Kerr bound [7].

Despite the wealth of circumstantial evidence, there is no definite observational proof of the existence of astrophysical BHs. (A review and a critique of current evidence can be found in Refs. [2,8], respectively. See also Ref. [9] for a stimulating minireview.) Astrophysical objects without event horizon, yet observationally indistinguishable from BHs, cannot be excluded *a priori*.

Dark energy stars or ''gravastars'' are compact objects with de Sitter interior and Schwarzschild exterior [10,11]. These two regions are glued together around the would-be horizon by an ultrastiff thin shell. In this model, a gravitationally collapsing star undergoes a phase transition that prevents further collapse. The thickness of the shell sets an upper limit to the mass of the gravastar [11–13]. (A thorough analysis of the maximum compactness of gravastars can be found in Ref. [14].) Generalizations of the original model use a Born-Infeld phantom field [15], dark energy equation of state [16], or nonlinear electrodynamics [17]. Models without shells or discontinuities have been investigated in Ref. [18].

Boson stars are macroscopic quantum states which are prevented from undergoing complete gravitational collapse by the Heisenberg uncertainty principle [19,20]. Their models differ in the scalar self-interaction potential [21] and can be divided into three classes [22].

Miniboson stars.—If the scalar field is noninteracting, the maximum boson star mass is $M_{\max} \sim 0.633 m_{\rm Planck}^2/m$ [19]. This value is much smaller than the Chandrasekhar mass for fermion stars, $M_{\rm Ch} \sim m_{\rm Planck}^3/m^2$. Stability of supermassive objects requires an ultralight boson of mass $m = 8.45 \times 10^{-26}$ GeV $(10^6 M_\odot/M_{\max})$.

Massive boson stars.—The requirement of ultralight bosons can be lifted if the scalar field possesses a quartic self-interaction potential of the form $\lambda|\phi|^4/4$ [23]. As long as the coupling constant λ is much larger than

[*]Presently at CENTRA, Department de Física, Instituto Superior Técnico, Avenida Rovisco Pais 1, 1049-001 Lisboa, Portugal.
vcardoso@phy.olemiss.edu
[+]paolo.pani@ca.infn.it
[‡]mariano.cadoni@ca.infn.it
[§]cavaglia@phy.olemiss.edu

$(m/m_{\rm Planck})^2$, the maximum boson star mass can be of the order of the Chandrasekhar mass or larger, $M_{\rm max} \sim 0.062\lambda^{1/2} m^3_{\rm Planck}/m^2$. Thus supermassive objects may exist. Boson mass and coupling constant are related by $m = 3.2 \times 10^{-4}$ GeV $\lambda^{1/4}$ $(10^6 M_\odot/M_{\rm max})^{1/2}$.

Nontopological soliton stars.—If the self-interaction takes the form $U = m^2|\phi|^2(1 - |\phi|^2/\phi_0^2)^2$, compact nondispersive solutions with a finite mass may exist even in the absence of gravity [24]. The critical mass of these objects is $M_{\rm max} \sim 0.0198 m^4_{\rm Planck}/(m\phi_0^2)$. If $\phi_0 \sim m$, a star of mass $M \sim 10^6 M_\odot$ corresponds to a heavy boson of mass $m \sim 500$ GeV.

Boson stars are indistinguishable from BHs in the Newtonian regime. Since they are very compact, deviations in the properties of orbiting objects occur close to the Schwarzschild radius and are not easily detectable electromagnetically [25,26]. If the scalar field interacts only gravitationally with matter, compact objects may safely inspiral ''inside'' the boson star, the only difference with a BH being the absence of an event horizon [27]. Lack of strong constraints on boson masses makes these models difficult to rule out.

Gravastars and boson stars provide viable alternatives to astrophysical BHs. To ascertain the true nature of ultracompact objects, it is thus important to devise observational tests to distinguish these ultracompact objects from ordinary BHs. The traditional way to distinguish a BH from a neutron star is to measure its mass. If the latter is larger than the Chandrasekhar limit, the object is believed to be a BH. However, this method cannot be used for the ultracompact objects discussed above, because of their broad mass spectrum. A possibility is to look for observables related to the accretion mechanism. For example, the luminosity of quiescent BHs is lower than the maximum luminosity which is allowed by the gas present in their environment [28]. If the BH accretion rate is much smaller than the Eddington rate, the radiative efficiency is also very small [29]. Another possibility is to exploit the absence of a boundary layer at the surface. Compact stars with accretion disks have typically a narrow viscous boundary layer near their surface, which allows the release of a considerable amount of heat energy. On the other hand, if the central object is a BH, no boundary layer is formed. Arguments of this kind have already excluded many gravastar candidates [30]. Absence of type I x-ray bursts is another powerful indicator of the presence of a BH. Several studies on type I bursts show that they are produced when gas accretes on the surface of a neutron star [31], which then undergoes a semiregular series of thermonuclear explosions. Since BHs do not have surfaces, the surrounding gas cannot accumulate and thermonuclear instabilities do not develop.

Another very promising observational method to probe the structure of ultracompact objects is gravitational-wave astronomy [32]. Gravitational-wave detectors such as LIGO [33], VIRGO [34], TAMA [35], or LISA [36] could provide an efficient way to study these objects without intervening effects due to the interstellar medium. For example, the inspiral process of two compact objects allows a precise determination of their mass [37] and multipole moments [27,38–40]. The gravitational waveform in the presence of a surface is also expected to be different than the waveform in the presence of an event horizon [41]. A first study on the distinctive features of the inspiral signal of boson stars can be found in Ref. [42]. Detection of gravitational resonant modes due to the gravitational potential well could also provide a test for the presence of a horizon [22,43]. Preliminary studies for gravastars indicate that this method may be very efficient if the source is not too far away and gravitational-wave production is significant [13,22,44].

In this paper, we propose a new method for discriminating BHs from ultracompact horizonless objects and apply it to gravastars and bosons stars. Our method uses the fact that compact rotating objects without event horizon are unstable when an ergoregion is present. The origin of this *ergoregion instability* can be traced back to superradiant scattering. In a scattering process, superradiance occurs when scattered waves have amplitudes larger than incident waves. This leads to extraction of energy from the scattering body [45–47]. Instability may arise whenever this process is allowed to repeat itself ad infinitum. This happens, for example, when a BH is surrounded by a ''mirror'' that scatters the superradiant wave back to the horizon, amplifying it at each scattering. The total extracted energy grows exponentially with time until the radiation pressure destroys the mirror in a process called *BH bomb* (see Refs. [48,49]). If the mirror is inside the ergoregion, superradiance may lead to an inverted BH bomb. Some superradiant waves escape to infinity carrying positive energy, causing the energy inside the ergoregion to decrease and eventually generating an instability. This may occur for any rotating star with an ergoregion: The mirror can be either its surface or, for a star made of matter noninteracting with the wave, its center. BHs are stable, which could be due to the absorption by the event horizon being larger than superradiant amplification.

The ergoregion instability appears in any system with ergoregions and no horizons [50]. (See also Ref. [51] for an exhaustive discussion.) Explicit computations for ordinary rotating stars can be found in Refs. [52,53], where typical instability time scales are shown to be larger than the Hubble time. In this case, the ergoregion instability is too weak to produce any effect on the evolution of the star. This conclusion changes drastically for ultracompact stars. For compactness $M \gtrsim 0.5R$ and angular momentum $J \gtrsim 0.4M^2$, we find that instability time scales range approximately from 0.1 seconds to 1 week for objects with mass in the range $M \sim 1M_\odot$ to $10^6 M_\odot$, further decreasing for larger rotation rates.

Because of the difficulty of handling gravitational perturbations for rotating objects, the calculations below are

mostly restricted to scalar perturbations. However, we are able to show that the equation for axial gravitational perturbations of gravastars is identical to the equation for scalar perturbations in the large $l = m$ limit. There are also generic arguments suggesting that the time scale of gravitational perturbations is smaller than the time scale of scalar perturbations for low m. Thus our investigation seems to rule out some of these ultracompact, rapidly spinning objects as BH candidates.

This paper is organized as follows. In Sec. II we review the main characteristics of the ultracompact objects discussed above. Our discussion is nonexhaustive and strictly limited to concepts and tools which will be needed in the rest of the paper. Section II A introduces the two gravastar models which will be discussed in the subsequent analysis. Since there are no known solutions describing rotating gravastars, the formalism of Refs. [54,55] will be used to discuss rotating gravastars. Section II B introduces boson stars [23]. Numerical results for rotating boson stars are taken from Ref. [56]. Section III presents a detailed investigation of the instability of boson stars and gravastars using the WKB approximation. The WKB analysis is then compared with full numerical results obtained by direct integration of the Klein-Gordon equation. Detectability of the ergoregion instability by gravitational-wave detectors is addressed in Sec. IV. Section V contains a brief discussion of the results and concludes the paper.

Geometrized units ($G = c = 1$) are used throughout the paper, except when numerical results for rotating boson stars from Ref. [56] are discussed (Sec. II B). In this case, the Newton constant is defined as $G = 0.05/(4\pi)$.

II. STRUCTURE OF ULTRACOMPACT ASTROPHYSICAL OBJECTS

This section discusses the main properties of gravastars and boson stars. The derivation of nonrotating solutions is partly based on Refs. [11,13,23,56].

A. Gravastars

Although exact solutions for spinning gravastars are not known, they can be studied in the limit of slow rotation by perturbing the nonrotating solutions [54]. This procedure was used in Ref. [55] to study the existence of ergoregions for ordinary rotating stars with uniform density. Their analysis is repeated below for gravastars. In the following, we discuss the original thin-shell model by Mazur and Mottola [11] and the anisotropic fluid model by Chirenti and Rezzolla [13,18].

1. Nonrotating thin-shell model

In this model, the spacetime

$$ds^2 = -f(r)dt^2 + B(r)dr^2 + r^2 d\Omega_2^2 \tag{2.1}$$

consists of three regions:

$$\begin{aligned} &\text{I. Interior: } 0 \le r \le r_1, && \rho = -p, \\ &\text{II. Shell: } r_1 \le r \le r_2, && \rho = p, \\ &\text{III. Exterior: } r_2 \le r, && \rho = p = 0, \end{aligned} \tag{2.2}$$

where ρ is the energy density and p is the isotropic pressure of the gravastar. In region I, $\rho = 3H_0^2/8\pi$ is constant and the metric is de Sitter:

$$f = \frac{C}{B} = C(1 - H_0^2 r^2), \qquad 0 \le r \le r_1, \tag{2.3}$$

where C is an integration constant to be determined from matching conditions. In region III the spacetime is described by the Schwarzschild metric,

$$f = \frac{1}{B} = 1 - \frac{2M}{r}, \qquad r_2 \le r. \tag{2.4}$$

In region II, the metric is determined by the system of equations,

$$d\ln r = \frac{dh}{1 - w - h}, \qquad h \equiv \frac{1}{B} \tag{2.5}$$

$$d\ln h = -\left(\frac{1 - w - h}{1 + w - 3h}\right) d\ln w, \tag{2.6}$$

where $w = 8\pi r^2 p$ and $wf/r^2 =$ constant. A simple analytical solution can be obtained for a thin shell [11]. In the limit $r_1 \to r_2$, one obtains

$$\frac{1}{B} \simeq \epsilon \frac{(1 + w)^2}{w} \ll 1, \tag{2.7}$$

where ϵ is an integration constant. The continuity of the metric coefficients f and B at r_1 and r_2 implies that ϵ, C, M, and H_0 are related to r_1, r_2, $w_1 \equiv w(r_1)$, and $w_2 \equiv w(r_2)$ by [13]

$$\epsilon = -\ln\frac{r_2}{r_1}\left(\ln\frac{w_2}{w_1} - \frac{1}{w_2} + \frac{1}{w_1}\right)^{-1}, \tag{2.8}$$

$$C = \left(\frac{1 + w_2}{1 + w_1}\right)^2, \tag{2.9}$$

$$M = \frac{r_2}{2}\left[1 - \frac{\epsilon(1 + w_2)^2}{w_2}\right], \tag{2.10}$$

$$H_0^2 = \frac{1}{r_1^2}\left[1 - \frac{\epsilon(1 + w_1)^2}{w_1}\right]. \tag{2.11}$$

The above relations and Eq. (2.5) completely determine the structure of the gravastar. A typical solution is shown in the upper panel of Fig. 1 for $r_2 = 1.05$, $r_1 = 1$, $w_1 = 350$, and $w_2 = 1$.

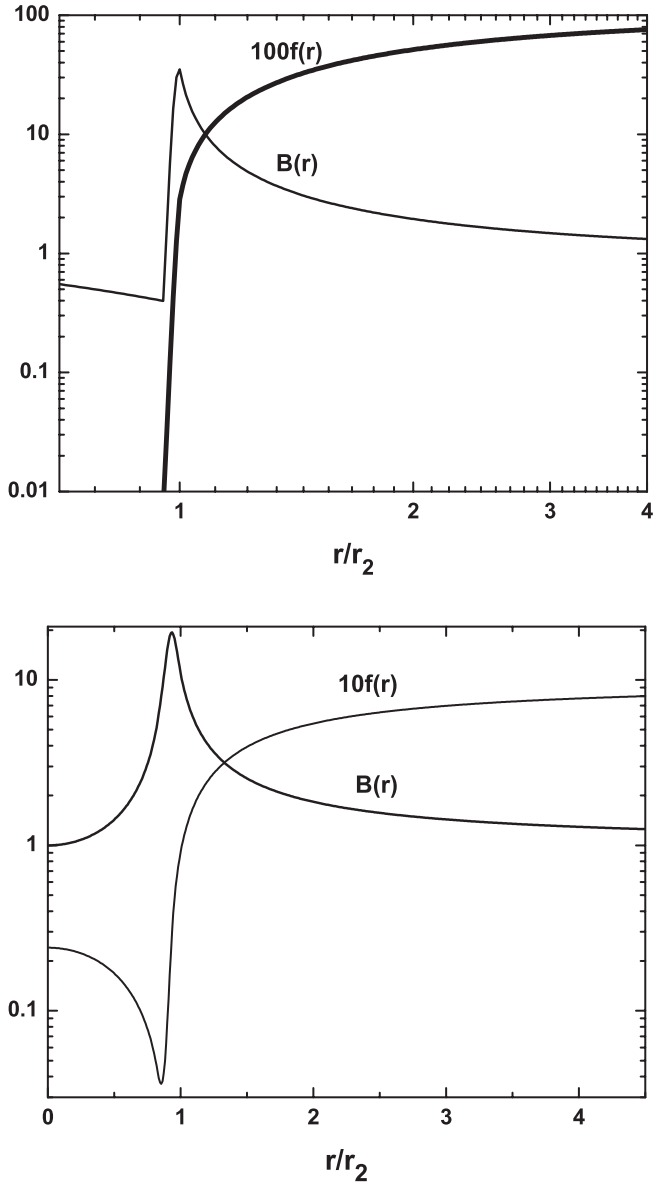

FIG. 1. Top panel: Metric coefficients for the thin-shell model gravastar with $r_2 = 1.05$, $r_1 = 1$, $w_1 = 350$, and $w_2 = 1$, corresponding to $M \sim 0.485 r_2$. Bottom panel: Anisotropic pressure model for $r_2 = 2.2$, $r_1 = 1.8$, and $M = 1$, corresponding to $M \sim 0.45 r_2$.

2. Nonrotating gravastars with anisotropic pressure

This model assumes a thick shell with continuous profile of anisotropic pressure to avoid the introduction of an infinitesimally thin shell. The stress-energy tensor is $T^{\mu}{}_{\nu} = \mathrm{diag}[-\rho, p_r, p_t, p_t]$, where p_r and p_t are the radial and tangential pressures, respectively. The density function is

$$\rho(r) = \begin{cases} \rho_0, & 0 \le r \le r_1 \quad \text{region I} \\ ar^3 + br^2 + cr + d, & r_1 < r < r_2 \quad \text{region II} \\ 0, & r_2 \le r \quad \text{region III} \end{cases}$$

with boundary conditions $\rho(0) = \rho(r_1) = \rho_0$, $\rho(r_2) = \rho'(r_1) = \rho'(r_2) = 0$, and

$$a = \frac{2\rho_0}{(r_2 - r_1)^3}, \qquad b = -\frac{3\rho_0(r_2 + r_1)}{(r_2 - r_1)^3}, \tag{2.12}$$

$$c = \frac{6\rho_0 r_1 r_2}{(r_2 - r_1)^3}, \qquad d = \frac{\rho_0(r_2^3 - 3r_1 r_2^2)}{(r_2 - r_1)^3}. \tag{2.13}$$

The density is related to the total mass M by

$$\frac{\rho_0}{M} = \frac{15}{2\pi(r_1 + r_2)(2r_1^2 + r_1 r_2 + 2r_2^2)}. \tag{2.14}$$

The radial pressure p_r is chosen as [13]

$$p_r(\rho) = \left(\frac{\rho^2}{\rho_0}\right)\left[\alpha - (1 + \alpha)\left(\frac{\rho}{\rho_0}\right)^2\right], \tag{2.15}$$

where the parameter α is determined by demanding that the maximum sound speed coincides with the speed of light. (This requirement rules out superluminal behavior and implies $\alpha \sim 2.21$.) The metric coefficients are

$$f = \left(1 - \frac{2M}{r_2}\right)e^{\Gamma(r) - \Gamma(r_2)}, \qquad \frac{1}{B} = 1 - \frac{2m(r)}{r}, \tag{2.16}$$

where

$$m(r) = \int_0^r 4\pi r^2 \rho dr,$$

and

$$\Gamma(r) = \int_0^r \frac{2m(r) + 8\pi r^3 p_r}{r(r - 2m(r))} dr. \tag{2.17}$$

The above equations completely determine the structure of the gravastar. Both the metric and its derivatives are continuous across r_2 and throughout the spacetime. The behaviors of the metric coefficients for a typical gravastar are shown in the bottom panel of Fig. 1.

3. Slowly rotating rigid gravastars and ergoregions

There are no known solutions describing rotating gravastars. Thus an analysis of the ergoregion instability for these objects is nontrivial. Fortunately, slowly rotating solutions can be obtained using the formalism developed in Ref. [54], which we now extend to the case of anisotropic stresses.

A rotation of order Ω gives corrections of order Ω^2 in the diagonal coefficients of the metric (2.1) and introduces a nondiagonal term of order Ω,

$$g_{t\phi} \equiv -\zeta g_{\phi\phi}, \tag{2.18}$$

where ϕ is the azimuthal coordinate. The metric coefficient $g_{t\phi}$ defines the angular velocity of frame dragging $\zeta = \zeta(r)$. The full metric is

$$ds^2 = -f(r)dt^2 + B(r)dr^2 + r^2 d\theta^2 + r^2\sin^2\theta(d\phi - \zeta(r)dt)^2. \quad (2.19)$$

We consider the anisotropic fluid stress-energy tensor

$$T^{\mu\nu} = (\rho + p_t)U^\mu U^\nu + p_t g^{\mu\nu} + (p_r - p_t)s^\mu s^\nu, \quad (2.20)$$

where

$$U^\mu U_\mu = -1, \qquad s^\mu s_\mu = 1, \qquad U^\mu s_\mu = 0,$$
$$U^r = U^\theta = 0, \qquad U^\phi = \Omega U^t,$$
$$U^t = [-(g_{tt} + 2\Omega g_{t\phi} + \Omega^2 g_{\phi\phi})]^{-1/2}.$$

Equation (2.20) describes an anisotropic fluid with radial pressure p_r and tangential pressure p_t, rotating with angular velocity Ω as measured by an observer at rest in the (t, r, θ, ϕ) coordinates. If the gravastar rotates rigidly, i.e. Ω = constant, the Einstein equations at order ζ give

$$-8\pi\rho = \frac{B - B^2 - rB'}{r^2B^2}, \quad (2.21)$$

$$8\pi p_r = \frac{f - Bf + rf'}{r^2Bf}, \quad (2.22)$$

$$8\pi p_t = -\frac{2f^2B' + rBf'^2}{4rB^2f^2} - \frac{f(rB'f' - 2B(f' + rf''))}{4rB^2f^2}. \quad (2.23)$$

An equation for $\zeta(r)$ is obtained by considering

$$R_{t\phi} = 8\pi\left(T_{t\phi} - \frac{1}{2}g_{t\phi}T\right). \quad (2.24)$$

Using Eqs. (2.21) and (2.22), Eq. (2.24) is written as

$$\zeta'' + \zeta'\left(\frac{4}{r} + \frac{j'}{j}\right) = 16\pi B(r)(\zeta - \Omega)(\rho + p_t), \quad (2.25)$$

where $j \equiv (fB)^{-1/2}$ is evaluated at zeroth order and ρ, p_t are given in terms of the nonrotating geometry by Eqs. (2.21) and (2.23), respectively. The above equation reduces to the corresponding equation in Ref. [54] for isotropic fluids. Solutions of Eq. (2.25) describe rotating gravastars to first order in Ω.

Spinning gravastars may possess ergoregions. A simple but general procedure to determine their presence for slowly rotating stars is described in Ref. [55]. This method requires only a knowledge of the metric of nonrotating objects and compares favorably with more sophisticated numerical analyses [57].

The ergoregion can be found by computing the surface on which g_{tt} vanishes [55]:

$$0 = -f(r) + \zeta^2 r^2\sin^2\theta. \quad (2.26)$$

Equation (2.26) is expected to be a good approximation to the location of the ergoregion specially for very compact stars [55]. The solution of Eq. (2.26) is topologically a torus. In the equatorial plane we have

$$r\zeta(r) = \sqrt{f(r)}. \quad (2.27)$$

The existence and the boundaries of the ergoregions can be computed from the above equations. Equation (2.25) is integrated from the origin with initial conditions $(\Omega - \zeta)' = 0$ and $(\Omega - \zeta)$ finite. Changing the value of $(\Omega - \zeta)$, the whole space of slowly rotating gravastars can be obtained. The exterior solution satisfies $\Omega - \zeta = \Omega(1 - 2I/r^3)$, where I is the moment of inertia of the star. Demanding the continuity of both $(\Omega - \zeta)'$ and $(\Omega - \zeta)$, ζ and I are uniquely determined. The rotation parameter Ω depends on the initial condition at the origin.

Figure 2 shows the results for three different gravastars described in the previous sections. The minima of the curves are the minimum values of J/M^2 which are required for the existence of the ergoregion. Comparison with the results for stars of uniform density [55] shows that ergoregions form more easily around gravastars due to their higher compactness. Figure 2 also shows that the ergoregions spread inside the gravastar. (The ergoregion can be located by drawing a horizontal line at the desired value of J/M^2, as explained in the caption.)

Gravastars spinning above a given threshold are not stable against mass shedding [58]. Instability arises when the centrifugal force is strong enough to disrupt the star. In Newtonian gravity, the equatorial mass shedding frequency is approximately the Keplerian frequency $M\Omega_K = (M/R)^{3/2}$. Although corrections to the Keplerian frequency are expected in a general relativistic framework, Ω_K provides a good estimator for the validity of the slow-rotation approximation. (See Ref. [59] for a comparison of the slow-rotation regime vs full numerical results.) In the following, the slow-rotation approximation will be considered valid for $\Omega/\Omega_K < 1$. Numerical results extend up to $\Omega \sim \Omega_K$.

B. Boson stars

A well-known example of nonrotating boson star is the model by Colpi, Shapiro, and Wasserman (CSW) [23]. A variation of the CSW model which allows for rotating solutions is the Kleihaus, Kunz, List, and Schaffer (KKLS) model [56]. The KKLS solution is based on the self-interacting complex scalar field Φ with Lagrangian density

$$\mathcal{L}_{\mathrm{KKLS}} = -\tfrac{1}{2}g^{\mu\nu}(\Phi^*_{,\mu}\Phi_{,\nu} + \Phi^*_{,\nu}\Phi_{,\mu}) - U(|\Phi|), \quad (2.28)$$

where $U(|\Phi|) = \lambda|\Phi|^2(|\Phi|^4 - a|\Phi|^2 + b)$. The mass of the boson is given by $m_{\mathrm{B}} = \sqrt{\lambda b}$. The equations for the boson star structure can be solved by setting

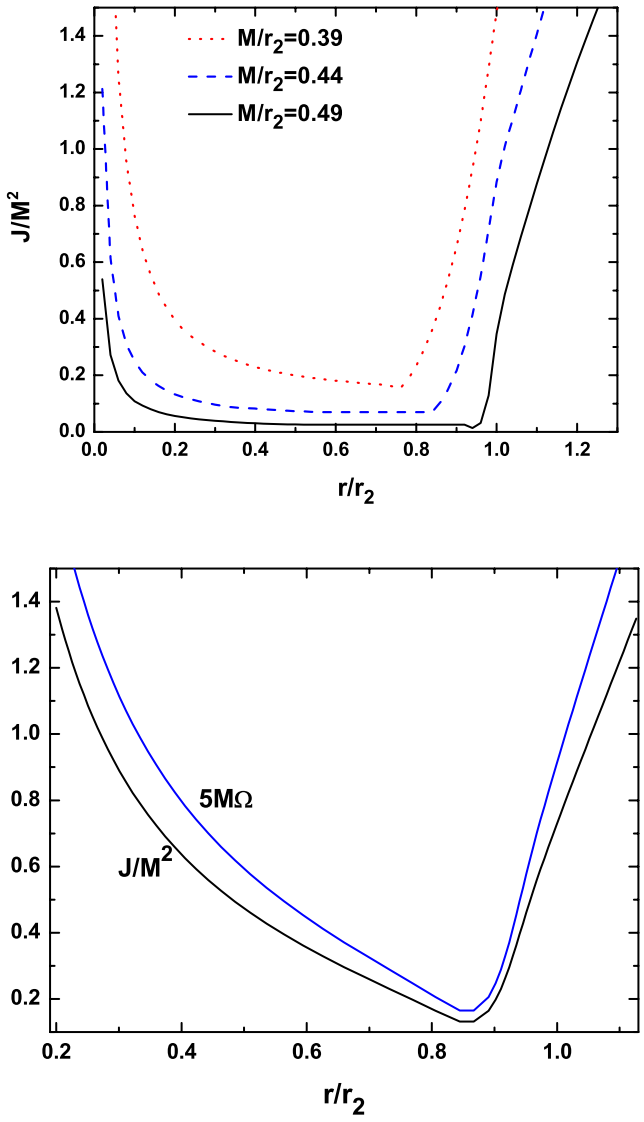

FIG. 2 (color online). Top panel: Size of the ergoregion for three different gravastars in the thin-shell limit. The vertical axis gives the angular momentum of the gravastar in units of its total mass. The horizontal axis gives the locations of the ergoregion boundaries in units of the gravastar radius r_2. Each curve refers to a different gravastar. The minima of the curves determine the existence and extent of ergoregions. The size of an ergoregion can be found by drawing a horizontal line at a given value of J/M^2; its intersections with the curves give the radii of the ergoregion boundaries. From top to bottom the three curves refer to $r_2 = 1.3$, $r_1 = 1$, $w_1 = 50$n and $w_2 = 1$, corresponding to $M \sim 0.39 r_2$; $r_2 = 1.2$, $r_1 = 1$, $w_1 = 150$, and $w_2 = 1$, corresponding to $M \sim 0.44 r_2$; $r_2 = 1.05$, $r_1 = 1$, $w_1 = 350$, and $w_2 = 1$, corresponding to $M \sim 0.49 r_2$. Bottom panel: J/M^2 and angular frequency Ω for the anisotropic pressure model with $r_2 = 2.2$, $r_1 = 1.8$, and $M = 1$. The angular frequency is always very small, thus the slow-rotation formalism applies. These results extend up to the Keplerian frequency Ω_K.

$$ds^2 = -f dt^2 + \frac{k}{f}[g(dr^2 + r^2 d\theta^2) + r^2 \sin^2\theta (d\varphi - \zeta(r) dt)^2] \quad (2.29)$$

and $\Phi = \phi e^{i\omega_s t + in\varphi}$, where the metric components and the real function ϕ depend only on r and θ. The requirement that Φ is single valued implies $n = 0, \pm 1, \pm 2, \ldots$. The solution has spherical symmetry for $n = 0$ and axial symmetry otherwise. The mass M and the angular momentum J can be read off from the asymptotic expansion of f and ζ,

$$M = \frac{1}{2G} \lim_{r\to\infty} r^2 \partial_r f, \qquad J = \frac{1}{2G} \lim_{r\to\infty} r^3 \zeta, \quad (2.30)$$

respectively. Since the Lagrangian density is invariant under a global $U(1)$ transformation, the current $j^\mu = -i\Phi^* \partial^\mu \Phi + \text{c.c.}$ is conserved. The associated charge is

$$Q = 4\pi\omega_s \int_0^\infty \int_0^\pi |g|^{1/2} \frac{1}{f}\left(1 + \frac{n}{\omega_s}\frac{\omega}{r}\right)\phi^2 dr d\theta. \quad (2.31)$$

It can be shown that the angular momentum J and the scalar charge Q of stationary solutions, i.e., solutions with a timelike and rotational Killing vector, are related by the quantization condition $J = nQ$ [60]. This may erroneously lead to the conclusion that boson stars are gravitationally stable because a continuous extraction of angular momentum is needed to trigger instability. However, the above quantization condition applies for objects for which such Killing vectors can be defined and we will assume that this condition is broken in the presence of perturbations. In this case, an arbitrary amount of angular momentum can be extracted and it will be shown below that gravitational-wave emission leads to an instability on very short time scales.

The numerical procedure to extract the metric and the scalar field is described in Ref. [56]. Throughout the paper we will consider solutions with $n = 2$, $b = 1.1$, $\lambda = 1.0$, $a = 2.0$ and different values of $(J, M) = (3781, 1296)$, $(3400, 1081)$, $(2800, 906)$, corresponding to $J/(\mathrm{GM}^2) \sim 0.566$, 0.731, and 0.858, respectively. The $n = 1$ solutions in Ref. [56] exhibit similar features. The two top panels of Fig. 3 show the metric functions for boson stars with $J/(\mathrm{GM}^2) \sim 0.566$ and 0.858 along the equatorial plane. The change in the metric potentials from $\theta = \pi/2$ to $\theta = \pi/4$ for these solutions is plotted in the bottom panels of Fig. 3. The metric functions do not depend significantly on the longitudinal angle. Figure 4 gives g_{tt} as a function of distance for the case with $J/(\mathrm{GM}^2) \sim 0.566$ at the equator. The behavior of g_{tt} demonstrates that boson stars develop ergoregions deeply inside the star. For this particular choice of parameters, the ergoregion extends from $r/(\mathrm{GM}) \sim 0.0471$ to 0.770. A more complete discussion on the ergoregions of rotating boson stars can be found in Ref. [56].

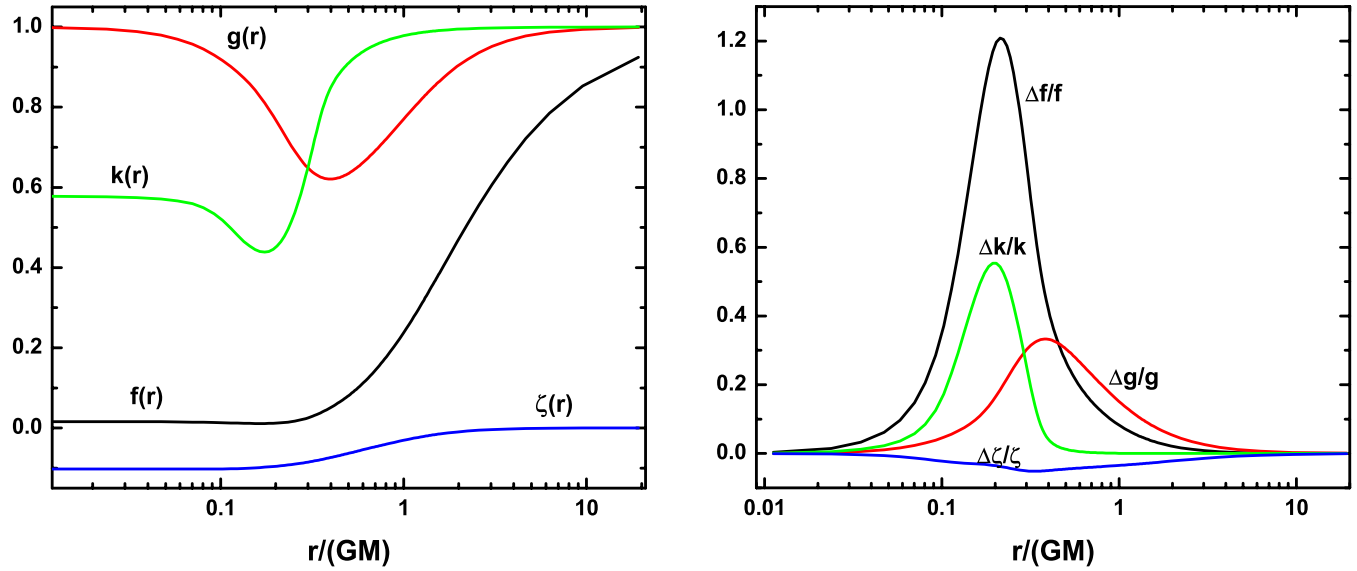

FIG. 3 (color online). Left panel: Metric coefficients for a rotating boson star along the equatorial plane, with parameters $n = 2$, $b = 1.1$, $\lambda = 1.0$, $a = 2.0$, $J/(\mathrm{GM}^2) \sim 0.566$. Right panel: Fractional difference of the metric potentials between $\theta = \pi/2$ and $\theta = \pi/4$ for the same star. The plot gives the maximum possible fractional difference between these quantities.

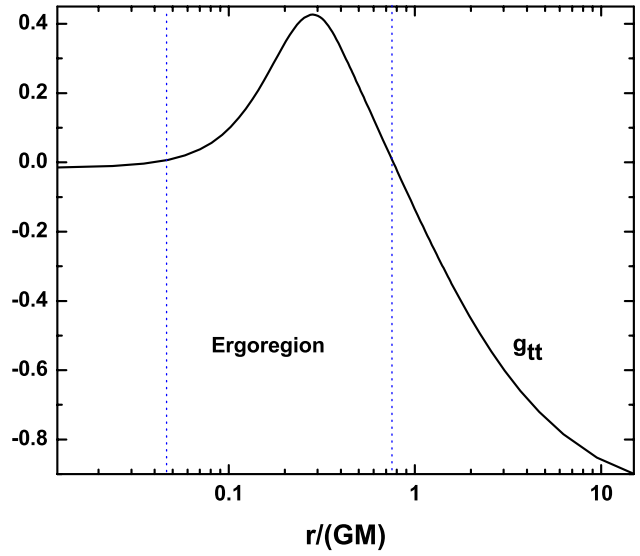

FIG. 4 (color online). The g_{tt} metric coefficient for a boson star with $J/(\mathrm{GM}^2) \sim 0.566$ at its equator. The ergoregion is identified by the region inside the dotted vertical lines and extends from $r/(\mathrm{GM}) \sim 0.047$ to 0.770.

III. ERGOREGION INSTABILITY FOR ROTATING STARS

The stability of ultracompact objects can be studied perturbatively by considering small deviations around equilibrium. As explained in the Introduction, we consider only scalar perturbations. This is justified as follows. Axial gravitational perturbations are described in the large $l = m$ limit by the same equation of scalar perturbations. In this regime, our results describe both kinds of perturbations. In the small $l = m$ limit, gravitational perturbations are expected to have shorter growth times than scalar perturbations: black holes are characterized by a superradiant amplification of spin-2 fields which is much stronger than the superradiant amplification of other fields. This is due to the potential barrier outside the horizon having different behavior for different spin-field s. Since the ultracompact objects we are dealing with are also characterized by a relativistic potential barrier, gravitational perturbations are expected to couple more strongly to the ergoregion and have smaller instability time scales. This conclusion is also verified under certain simplifying assumptions in Ref. [61]. Thus, scalar perturbations should provide a lower bound on the strength of the instability.

A. Axial gravitational perturbations for perfect fluid stars

In the large $l = m$ regime, axial gravitational perturbations [61,62] are described by a simple equation. In general, axial and polar perturbations are coupled when rotation is included [63]. For simplicity, we will assume that the zeroth-order polar perturbations vanish and there is no coupling. The full metric is a perturbation of Eq. (2.19) [63]:

$$ds^2 = ds_0^2 + 2\sum_{lm}(h_0^{lm}(t,r) + h_1^{lm}(t,r)) \times (-\sin^{-1}\theta\partial_\phi Y_{lm}d\theta + \sin\theta\partial_\theta Y_{lm}d\phi), \quad (3.1)$$

where ds_0^2 is the unperturbed metric (2.19) and Y_{lm} are scalar spherical harmonics. The quantities

$$h_0^{lm} \equiv \sqrt{f(r)/B(r)}K_6, \qquad h_1^{lm} \equiv \sqrt{B(r)/f(r)}V_4, \quad (3.2)$$

satisfy the system of equations [see Eqs. (13)–(16) in Ref. [62]]

$$K_3' = 16\pi(p+\rho)u_3 - \frac{2K_3}{r} + \frac{l^2+l-2}{r^2}K_6 - \frac{2m\zeta' V_4}{(l^2+l)f}, \tag{3.3}$$

$$K_6' = -\frac{B}{f}(-\omega+m\zeta)V_4 - \left(\frac{f'}{2f} - \frac{B'}{2B} - \frac{2}{r}\right)K_6 + BK_3, \tag{3.4}$$

where K_3 and K_6 are two extrinsic curvature variables and

$$V_4 = \frac{r^2}{l^2+l-2}\left((-\omega+m\zeta)K_3 - \frac{2m\zeta'}{l(l+1)}\frac{K_6}{B}\right), \tag{3.5}$$

$$u_3 = \frac{2m(\Omega-\zeta)}{2m(\Omega-\zeta) - l(l+1)(-\omega+m\Omega)}K_6. \tag{3.6}$$

Here and throughout this paper, it is understood that $\omega \equiv \omega_{lm}$. In the large $l = m$ limit, Eqs. (3.3) and (3.4) reduce to

$$K_3' = -\frac{2}{r}K_3 + \frac{m^2}{r^2}K_6, \tag{3.7}$$

$$K_6' = BK_3 - \frac{B}{f}(\Sigma+\zeta)^2 r^2 K_3 - \left(\frac{f'}{2f} - \frac{B'}{2B} - \frac{2}{r}\right)K_6, \tag{3.8}$$

where $\Sigma \equiv -\omega/m$. Combining Eqs. (3.7) and (3.8) and neglecting terms of order $1/m^2$, it follows

$$K_3'' + m^2\frac{B}{f}\left((\Sigma+\zeta)^2 - \frac{f}{r^2}\right)K_3 = 0. \tag{3.9}$$

This equation also describes the scalar perturbations of gravastars, as it will be shown below.

B. Scalar field instability for slowly rotating gravastars: WKB approach

Consider now a minimally coupled scalar field in the background of a gravastar. The metric of gravastars is given by Eq. (2.19). In the large $l = m$ limit, which is appropriate for a WKB analysis [52,64], the scalar field can be expanded as

$$\Phi = \sum_{lm}\bar{\chi}_{lm}(r)\exp\left[-\frac{1}{2}\int\left(\frac{2}{r}+\frac{f'}{2f}+\frac{B'}{2B}\right)dr\right] \times e^{-i\omega t}Y_{lm}(\theta,\phi). \tag{3.10}$$

The functions $\bar{\chi}_{lm}$ are determined by the Klein-Gordon equation, which yields

$$\bar{\chi}_{lm}'' + m^2 T(r,\Sigma)\bar{\chi}_{lm} = 0, \tag{3.11}$$

where Σ is defined as below Eq. (3.8) and

$$T = \frac{B(r)}{f(r)}(\Sigma - V_+)(\Sigma - V_-), \tag{3.12}$$

$$V_\pm = -\zeta \pm \frac{\sqrt{f(r)}}{r}. \tag{3.13}$$

Equation (3.11) follows from Eq. (3.10) when terms of order $\mathcal{O}(1/m^2)$ are dropped. Equation (3.11) can be shown to be identical to Eq. (3.9) for the axial gravitational perturbations of perfect fluid stars. Therefore, the following results apply to both kinds of perturbations.

The eigenfrequencies of Eq. (3.11) can be computed in the WKB approach following Ref. [52]. This method is in excellent agreement with full numerical results [53,64]. The quasibound unstable modes are determined by

$$m\int_{r_a}^{r_b}\sqrt{T(r)}dr = \frac{\pi}{2} + n\pi, \qquad n = 0, 1, 2, \ldots \tag{3.14}$$

and have time scale

$$\tau = 4\exp\left[2m\int_{r_b}^{r_c}\sqrt{|T|}dr\right]\int_{r_a}^{r_b}\frac{d}{d\Sigma}\sqrt{T}dr, \tag{3.15}$$

where r_a, r_b are solutions of $V_+ = \Sigma$ and r_c is determined by the condition $V_- = \Sigma$.

The potentials $V_\pm$ are displayed in Fig. 5 for the gravastar models of Sec. II A. The top panel shows the potential for the thin-shell model with $r_2 = 1.3$, $r_1 = 1$, $w_1 = 50$, and $w_2 = 1$. The gravastar rotates with angular frequency $\Omega \sim 0.105$ and the ergoregion lies in the region $r \sim (0.247, 0.832)r_2$. The bottom panel refers to the anisotropic pressure model with $r_2 = 2.2$, $r_1 = 1.8$, and $M = 1$. The ergoregion extends from $r \sim 0.270r_2$ to $r \sim 1.055r_2$ and rotates with angular frequency $\Omega \sim 0.250$.

The results of the WKB computation are shown in Fig. 6 and Tables I, II, and III. Figure 6 displays the results for the least compact thin-shell gravastar of Sec. II A with $m = 1$, 4. Although the WKB approximation breaks down at low m values, these results still provide reliable estimates [52]. This claim will be verified in Sec. with a full numerical integration of the Klein-Gordon equation. Table I compares three different gravastars for $J/M^2 = 1$ and $m = 1, 2, \ldots 5$. The results show that the instability time scale decreases as the star becomes more compact. Table II refers to the most compact thin-shell gravastar for various angular frequencies. The instability time scale depends strongly on the rotation. A fit for the instability time scale in powers of J/M^2 yields

$$\log\tau/M \sim a + b\sqrt{J/M^2} + cJ/M^2, \tag{3.16}$$

where $a = 68.0$, $b = -76.7$, $c = 26.2$ for $m = 5$ and $a = 55.8$, $b = -61.4$, $c = 21.0$ for $m = 4$, respectively. The results for lower m values show similar behaviors. For instance, for $m = 1$ the coefficients are $a = 19.7$, $b = -16.2$, and $c = 5.6$. Table III shows the WKB results for the anisotropic pressure model for different values of

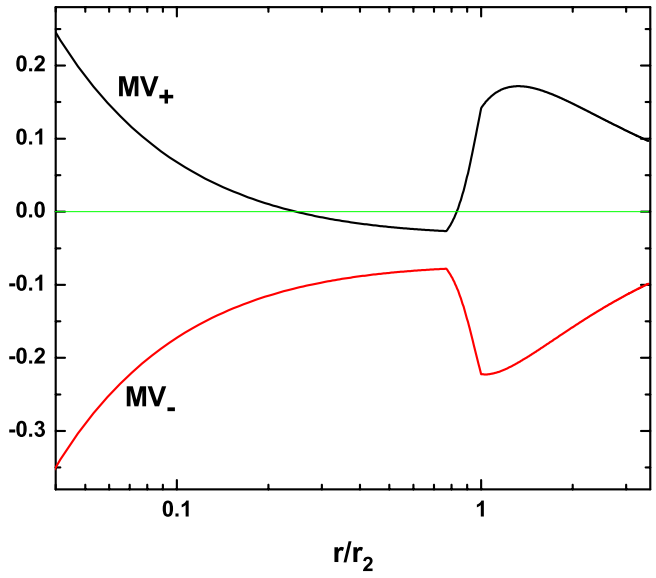

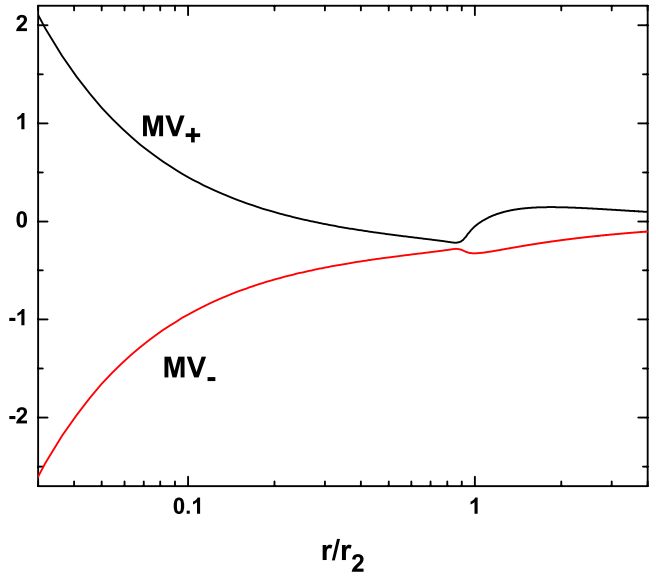

FIG. 5 (color online). Top panel: Potentials $V_{\pm}$ for the thin-shell gravastar with $r_2 = 1.3$, $r_1 = 1$, $w_1 = 50$, and $w_2 = 1$. The ergoregion extends from $r \sim 0.247 r_2$ to $0.832 r_2$ and corresponds to a gravastar with $J \sim 0.333 M^2$ and $M\Omega \sim 0.105$. Bottom panel: Potentials for the anisotropic pressure gravastar with $r_2 = 2.2$, $r_1 = 1.8$, and $M = 1$. The ergoregion extends from $r \sim 0.270 r_2$ to $r \sim 1.055 r_2$ and rotates with angular momentum $J/M^2 = 1.00$, corresponding to $\Omega \sim 0.250$.

J/M^2. Larger values of J/M^2 make the star more unstable. The instability time scales are fitted by

$$\log \tau/M \sim a + b(J/M^2)^c, \tag{3.17}$$

where $a = -21.9$, $b = 39.2$, $c = -0.39$ for $m = 5$ and $a = -13.7$, $b = 28.5$, $c = -0.43$ for $m = 4$. The trend for lower-m is similar. The coefficients for $m = 1$ are $a = 7.4$, $b = 0.57$, $c = -3.0$.

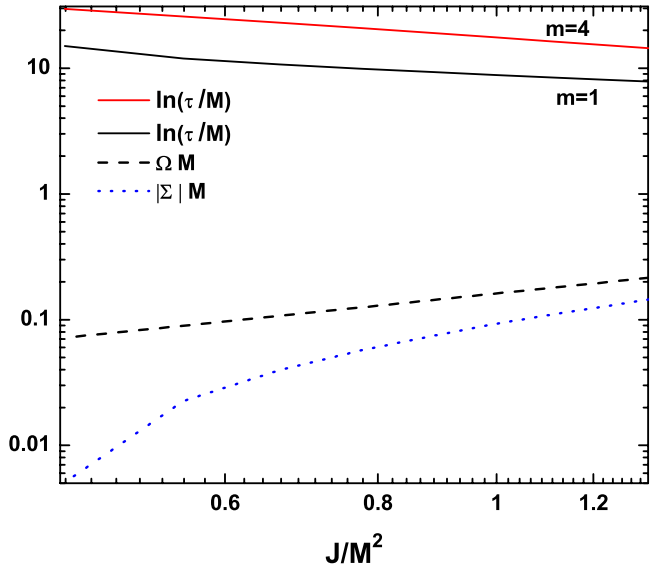

FIG. 6 (color online). Details of the ergoregion instability ($m = 1$ and $m = 4$) for the thin-shell gravastar of Sec. II A 1 with $r_2 = 1.3$, $r_1 = 1$, $w_1 = 50$, and $w_2 = 1$. The plot shows the logarithm of the dimensionless instability time scale τ/M, the dimensionless angular velocity $M\Omega$, and the oscillation frequency Σ vs the angular momentum per unit mass, J/M^2. The $m = 2, 3$ modes follow a similar pattern and are in between the $m = 1, 4$ results.

Both models have similar low-m behaviors. It will be shown in Sec. that the WKB results for the instability time scale differ from the numerical results by about 1 order of magnitude at low m. On the contrary, the resonant frequencies match well the WKB results even for low-m modes. Calculations show that the resonant frequency is $\mathrm{Re}(\omega) \sim \alpha\Omega$, where $\alpha \sim 1.1$–1.2.

The maximum growth time of the instability is of the order of a few thousand M, at least for large J. This instability is crucial for the star evolution. Comparison of Table V with Tables 1 and 2 of Ref. [52] shows that the ergoregion instability of gravastars is stronger than the ergoregion instability of uniform density stars by many orders of magnitude. This seems to be a general feature of all ultracompact objects discussed here. Gravitational perturbations are expected to be even more unstable.

TABLE I. WKB results for the instability of rotating thin-shell gravastars with $J/M^2 = 1$. The instability grows with compactness.

	$(-10^2 M\Sigma, \tau/M)$		
m	$r_2 = 1.3$	$r_2 = 1.2$	$r_2 = 1.05$
1	$9.2,\ 6.85 \times 10^3$	$17,\ 5.26 \times 10^3$	$23,\ 9.16 \times 10^3$
2	$11,\ 1.23 \times 10^5$	$18,\ 5.63 \times 10^4$	$23,\ 7.37 \times 10^4$
3	$12,\ 2.31 \times 10^6$	$18,\ 6.06 \times 10^5$	$23,\ 5.98 \times 10^5$
4	$12,\ 4.34 \times 10^7$	$18,\ 6.58 \times 10^6$	$23,\ 4.86 \times 10^6$
5	$12,\ 8.26 \times 10^8$	$18,\ 7.13 \times 10^7$	$23,\ 3.99 \times 10^7$

TABLE II. WKB results for the instability of rotating thin-shell gravastars with $r_2 = 1.05$ and $r_1 = 1.0$. The mass shedding limit corresponds to $\Omega/\Omega_K = 1$, where $\Omega_K = \sqrt{M/r_2^3}$.

	$(-10^2 M\Sigma, \tau/M)$						
	$J/M^2 = 0.40$	$J/M^2 = 0.50$	$J/M^2 = 0.60$	$J/M^2 = 0.70$	$J/M^2 = 0.80$	$J/M^2 = 0.90$	$J/M^2 = 1.0$
m	$\Omega/\Omega_K = 0.28$	$\Omega/\Omega_K = 0.35$	$\Omega/\Omega_K = 0.42$	$\Omega/\Omega_K = 0.50$	$\Omega/\Omega_K = 0.57$	$\Omega/\Omega_K = 0.64$	$\Omega/\Omega_K = 0.71$
1	$8.4,\ 1.19 \times 10^5$	$10,\ 6.28 \times 10^4$	$13,\ 3.70 \times 10^4$	$16,\ 2.38 \times 10^4$	$18,\ 1.64 \times 10^4$	$20,\ 1.19 \times 10^4$	$23,\ 9.15 \times 10^3$
2	$8.7,\ 1.13 \times 10^7$	$11,\ 3.24 \times 10^6$	$14,\ 1.15 \times 10^6$	$16,\ 4.82 \times 10^5$	$18,\ 2.31 \times 10^5$	$21,\ 1.24 \times 10^5$	$23,\ 7.38 \times 10^4$
3	$8.8,\ 1.08 \times 10^9$	$11,\ 1.68 \times 10^8$	$14,\ 3.59 \times 10^7$	$16,\ 9.86 \times 10^6$	$18,\ 3.30 \times 10^6$	$21,\ 1.30 \times 10^6$	$23,\ 5.97 \times 10^5$
4	$8.9,\ 1.04 \times 10^{11}$	$11,\ 8.75 \times 10^9$	$14,\ 1.13 \times 10^9$	$16,\ 2.03 \times 10^8$	$18,\ 4.69 \times 10^7$	$21,\ 1.37 \times 10^7$	$23,\ 4.86 \times 10^6$
5	$8.9,\ 1.01 \times 10^{13}$	$11,\ 4.58 \times 10^{11}$	$14,\ 3.59 \times 10^{10}$	$16,\ 4.16 \times 10^9$	$18,\ 6.75 \times 10^8$	$21,\ 1.45 \times 10^8$	$23,\ 3.98 \times 10^7$

TABLE III. WKB results for the instability of rotating anisotropic pressure gravastars with $r_2 = 2.2$, $r_1 = 1.8$, and $M = 1$.

	$(-10^2 M\Sigma, \tau/M)$						
	$J/M^2 = 0.40$	$J/M^2 = 0.50$	$J/M^2 = 0.60$	$J/M^2 = 0.70$	$J/M^2 = 0.80$	$J/M^2 = 0.90$	$J/M^2 = 1.0$
m	$\Omega/\Omega_K = 0.33$	$\Omega/\Omega_K = 0.41$	$\Omega/\Omega_K = 0.49$	$\Omega/\Omega_K = 0.57$	$\Omega/\Omega_K = 0.65$	$\Omega/\Omega_K = 0.74$	$\Omega/\Omega_K = 0.82$
1	$0.24,\ 1.33 \times 10^7$	$2.7,\ 1.13 \times 10^5$	$5.2,\ 2.78 \times 10^4$	$7.6,\ 1.15 \times 10^4$	$10,\ 5.99 \times 10^3$	$12,\ 3.58 \times 10^3$	$15,\ 2.34 \times 10^3$
2	$3.1,\ 8.25 \times 10^7$	$5.6,\ 6.20 \times 10^6$	$8.1,\ 1.14 \times 10^6$	$10,\ 3.13 \times 10^5$	$13,\ 1.11 \times 10^5$	$15,\ 4.81 \times 10^4$	$18,\ 2.33 \times 10^4$
3	$4.2,\ 1.31 \times 10^{10}$	$6.6,\ 5.44 \times 10^8$	$9.1,\ 5.65 \times 10^7$	$12,\ 9.40 \times 10^6$	$14,\ 2.25 \times 10^6$	$17,\ 6.82 \times 10^5$	$19,\ 2.45 \times 10^5$
4	$4.7,\ 2.50 \times 10^{12}$	$7.2,\ 5.13 \times 10^{10}$	$9.7,\ 2.95 \times 10^9$	$12,\ 3.10 \times 10^8$	$15,\ 4.81 \times 10^7$	$17,\ 1.02 \times 10^7$	$20,\ 2.73 \times 10^6$
5	$5.1,\ 5.06 \times 10^{14}$	$7.6,\ 4.99 \times 10^{12}$	$10,\ 1.59 \times 10^{11}$	$13,\ 9.82 \times 10^9$	$15,\ 1.02 \times 10^9$	$17,\ 1.52 \times 10^8$	$20,\ 3.07 \times 10^7$

Comparison with numerical results

Accurate computations of the instability require numerical solutions of the Klein-Gordon equation. However, the WKB approximation provides reliable estimates of the numerical results. The exact potential T of Eq. (3.13) is

$$\bar{T} = -\frac{l(l+1)B}{r^2} + \frac{B(\omega - m\zeta)^2}{f} + \frac{B'}{2rB} + \frac{B''}{4B} - \frac{5B'^2}{16B^2} - \frac{f'}{2rf} + \frac{B'f'}{8Bf} + \frac{3f'^2}{16f^2} - \frac{f''}{4f}. \tag{3.18}$$

The results of the numerical integration for the anisotropic pressure gravastar with $r_2 = 2.2$, $r_1 = 1.8$, $M = 1$, and $J/M^2 = 1$ are shown in Table IV.

TABLE IV. Comparison between analytical and numerical results for anisotropic pressure gravastars with $J/M^2 = 1$, $r_2 = 2.2$, $r_1 = 1.8$, and $M = 1$. The numerical results for the real part are in good agreement with the WKB results. The agreement is better for larger values of m. The imaginary parts agree within an order of magnitude.

	$(-10^2 \Sigma M, \tau/M)$		
m	Analytical (A)	Numerical (N)	$\lvert\frac{\Sigma_A - \Sigma_N}{\Sigma_A}\rvert$
1	$15.0,\ 2.34 \times 10^3$	$21.9,\ 2.47 \times 10^3$	31.5%
2	$18.0,\ 2.34 \times 10^4$	$18.6,\ 1.81 \times 10^5$	3.2%
3	$19.0,\ 2.49 \times 10^5$	$18.7,\ 2.53 \times 10^6$	1.6%
4	$19.6,\ 2.74 \times 10^6$	$19.0,\ 3.33 \times 10^7$	3.2%
5	$19.8,\ 3.07 \times 10^7$	$19.3,\ 3.76 \times 10^8$	2.6%

The WKB approximation for the real part of the frequency shows a remarkably good agreement with the numerical results even at low values of m. For any $m > 1$ this agreement is better than 5%. The instability time scale seems to be more sensitive to the details of the WKB integration, with a level of agreement similar to that reported in Ref. [53]. The above results show that the WKB approximation correctly estimates the instability time scale for all values of m within an order of magnitude.

C. Scalar field instability for rotating boson stars: WKB approach

Consider a scalar field Ψ minimally coupled to the rotating boson star geometry (not to be confused with the scalar field which makes up the star). Since the metric coefficients depend on r and θ, the Klein-Gordon equation cannot be reduced, in general, to a one-dimensional problem. Separation of variables can be achieved by requiring $g = 1$, $f = f(r, \pi/2)$, $k = k(r, \pi/2)$, and $\zeta = \zeta(r, \pi/2)$. These assumptions are justified as follows. First, the metric function g is very close to unity throughout the entire coordinate region, as can be seen in Fig. 3. Since the Klein-Gordon equation does not depend on the derivatives of g, it seems safe to set $g = 1$ in the whole domain. Second, the angular dependence of the metric coefficients is negligible for slow rotations. The largest variation for one revolution around the star is that of f, which is less than 100% for most cases (see Fig. 3). Moreover, this dependence is extremely weak for most of the values of r. Third, perturbations are localized around the equator in

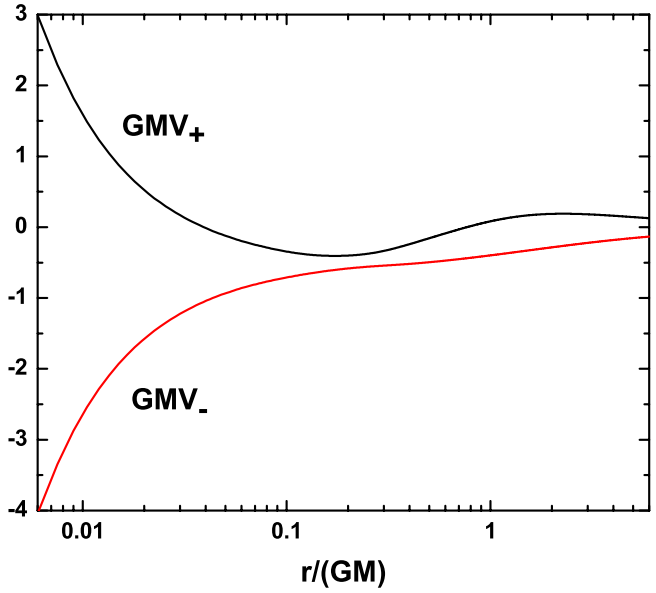

FIG. 7 (color online). Potentials $V_{\pm}$ for the boson star model with $J/(\mathrm{GM}^2) = 0.566$. The ergoregion extends from $r/(\mathrm{GM}) \sim 0.0478$ to 0.779.

the large $l = m$ behavior. Therefore, evaluating the metric coefficients at the equator may provide a reasonable approximation to the problem. The results obtained in this section are expected to give an order of magnitude estimate for the instability.

The equation for the scalar field is obtained by expanding the latter as

$$\Psi = \sum_{lm} \bar{\Psi}_{lm}(r) \exp\left[-\frac{1}{2}\int\left(\frac{2}{r} + \frac{k'}{k}\right)dr\right] e^{-i\omega t} Y_{lm}(\theta, \phi). \tag{3.19}$$

In the large $l = m$ limit, $\bar{\Psi}_{lm}$ is determined by

$$\bar{\Psi}''_{lm} + m^2 T(r, \Sigma)\bar{\Psi}_{lm} = 0, \tag{3.20}$$

where

$$T = \frac{k}{f^2}(\Sigma - V_+)(\Sigma - V_-), \tag{3.21}$$

TABLE V. Instability for rotating boson stars with parameters $n = 2$, $b = 1.1$, $\lambda = 1.0$, $a = 2.0$, and different values of J: $J/(\mathrm{GM}^2) = 0.566$, 0.731, and 0.858. The Newton constant is defined as $4\pi G = 0.05$.

	-10^2 GMΣ, $\tau/(\mathrm{GM})$		
m	$\frac{J}{\mathrm{GM}^2} = 0.566\,139$	$\frac{J}{\mathrm{GM}^2} = 0.730\,677$	$\frac{J}{\mathrm{GM}^2} = 0.857\,658$
1	31, 8.847×10^2	6.6, 6.303×10^3	-
2	36, 7.057×10^3	13, 5.839×10^4	0.68, 1.478×10^6
3	37, 6.274×10^4	16, $9.274. \times 10^5$	3.4, 2.815×10^8
4	38, 5.824×10^5	17, 1.603×10^7	4.9, 2.815×10^{10}
5	38, 5.554×10^6	18, 2.915×10^8	5.7, 1.717×10^{12}

$$V_{\pm} = \zeta \pm \frac{f}{r\sqrt{k}}, \qquad \Sigma \equiv \frac{\omega}{m}, \tag{3.22}$$

and terms of order $\mathcal{O}(1/m^2)$ have been neglected. The potentials $V_{\pm}$ are plotted in Fig. 7 for the rotating boson star with $J/(\mathrm{GM}^2) = 0.566$. The results of the WKB computation are summarized in Table V for $m = 1, 2, \ldots 5$. An interesting feature is that the instability time scale increases with the star angular momentum. Because of lack of sufficient numerical results, we do not yet know whether this behavior holds for all values of the angular momentum or the trend changes at some point. The maximum growth time for this boson star model is of the order of $10^6 M$ for $\frac{J}{\mathrm{GM}^2} = 0.857\,658$. This is a relatively short instability time scale, corresponding to about 1 s for a one solar-mass boson star.

IV. DETECTABILITY BY EARTH- AND SPACE-BASED GRAVITATIONAL-WAVE DETECTORS

The ergoregion instability may be of interest for gravitational-wave astronomy. Contrary to the r-mode instability of neutron stars [65,66], the ergoregion instability is not limited to solar-mass objects. Thus chances of detection are larger because the signal can fall in frequency bands where the detectors are more sensitive.

A. Signal-to-noise ratio

Detectability depends only on the energy released and the detector frequency bandwidth. The sky-averaged signal-to-noise ratio (SNR) is [67]

$$\rho^2 = \frac{2}{5\pi^2 D^2}\int df \frac{1}{f^2 S_h(f)}\frac{dE}{df}, \tag{4.1}$$

where D is the distance to the source and $S_h(f)$ is the noise power spectral density of the detector. Using $dE = 2\pi f dJ/m$, the SNR for the $l = m = 2$ mode, i.e. the mode for which the instability is expected to be stronger, is

$$\rho^2 = \frac{2}{5\pi D^2}\int df \frac{1}{f S_h(f)}\frac{dJ}{df}. \tag{4.2}$$

Equation (4.2) agrees with results in the literature [65,66,68] and is independent of the perturbation amplitude at lowest order. Higher-order corrections, however, would contain a dependence of the SNR ratio on the amplitude evolution. Fitting the resonant frequencies to

$$\mathrm{Re}[\omega] = 2\pi f \approx \alpha\Omega, \tag{4.3}$$

one finds $\alpha \sim 1.1$–1.2. From Eq. (4.3) it follows $dJ/df \approx 2\pi I/\alpha$. Assuming the moment of inertia $I \sim 2\beta M^3$ to be roughly independent of the angular velocity [65] (computations show that $\beta \sim 1$ for gravastars to a very good approximation), Eq. (4.2) can be rewritten as [65,66,68]

TABLE VI. SNR for ergoregion instability of an object at distance of 20 Mpc for LIGO/Advanced LIGO and LISA. (See text for details.)

			ρ			
$M/M_\odot$	10	20	30	40	50	100
LIGO	1	5	11	18	24	23
Advancecd LIGO	9	84	193	249	304	468

			ρ		
$M/M_\odot$	10^4	10^5	10^6	10^7	10^8
LISA	0.07	21	2428	1469	1417

$$\rho^2 = \frac{8\beta M^3}{5\alpha D^2}\int_{f_{\rm min}}^{f_{\rm max}} df\,\frac{1}{fS_h(f)}. \tag{4.4}$$

The minimum and maximum frequencies in the above integral are chosen as $f_{\rm min} = 0.9 f_{\rm max}$ (we here implicitly assume that the amplitude of the perturbation is sufficiently large so that $f_{\rm min}$ is reached within the typical operation time of a detector such as LIGO or LISA, i.e. $\sim$1 year). This is a conservative estimate based on a simple model for the evolution of the system. SNRs for objects at 20 Mpc distance for LIGO/Advanced LIGO and LISA are shown in Table VI for $\Omega M = 0.2$. Solar-mass objects are difficult to detect, although LIGO (Advanced LIGO) could be able to detect objects with $M \gtrsim 30M_\odot$ ($M \gtrsim 10M_\odot$). SNRs of several thousands are easily achieved for supermassive objects. These objects could be easily observed by LISA.

B. Waveforms

The expression for the SNR derived above is the optimal SNR. Search and detection techniques, i.e. matched filtering, usually require accurate theoretical templates. The derivation of accurate waveforms for the ergoregion instability is beyond the purpose of this paper. The physics involved is too complex and even the evolution of the instability itself is at present not known. The sole purpose of this section is to sketch the evolution of the most important quantities of the process.

The instability proceeds in two steps: A phase characterized by an exponential growth, where the linear approximation is valid, followed by a nonlinear phase. Contrary to the r-mode instability, the ergoregion instability does not couple strongly to the fluid composing the object. Therefore, the nonlinear phase is expected to be somewhat different from the r-mode saturation phase [65,66].

As an illustration of waveform estimation, consider the instability triggered by a particle in circular orbit around the compact object. Focusing on the $l = 2$ mode, the metric perturbations in the linear perturbation regime have the form

$$h_+ = \frac{M}{D}h_0 e^{t/\tau}\sin(\omega t - 2\phi)\chi_+, \tag{4.5}$$

$$h_\times = \frac{M}{D}h_0 e^{t/\tau}\cos(\omega t - 2\phi)\chi_\times, \tag{4.6}$$

where D is the distance to the source, $h_0 \ll 1$ and

$$\chi_+ \equiv \frac{\cos^2\theta + 1}{2}, \qquad \chi_\times \equiv \cos\theta. \tag{4.7}$$

The above waveforms mimic the Newtonian waveform produced by a small mass in circular orbit around the ultracompact object. The linear perturbation regime corresponds to $h_{+,\times} < 1$. The exact functional form of the waveform (4.7) is required to determine polarization and phase content of the waveform, but not the evolution of its amplitude.

From the discussion in the previous sections, the frequency of the wave is $\omega \sim \Omega(t)$. The time scale is $\tau \sim \tau_0(M\Omega)^{-6}$, where a dominant w-mode instability is assumed [61]. The mass can be determined as follows. The energy carried by the gravitational wave is [69]

$$\frac{d^2E}{dtd\Omega} = \lim_{D\to\infty}\frac{D^2}{16\pi}(\dot h_+^2 + \dot h_\times^2). \tag{4.8}$$

Assuming that all the energy carried by the gravitational wave is extracted from the star, it follows $dE/dt = -dM/dt$. The angular momentum radiated in the azimuthal mode m can be obtained from $dE = \omega dJ/m$. If this angular momentum is also completely extracted from the star, then $J = I\Omega$, where the moment of inertia $I = 2\beta M(t)^3$ is approximately constant in time. Setting $dJ/dt = m/\omega dE/dt = 2/(\alpha\Omega)dM/dt$, the mass variation rate is

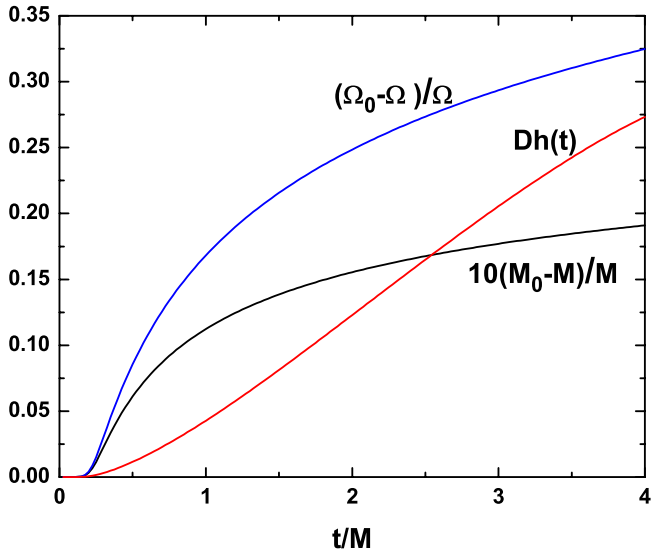

FIG. 8 (color online). Evolution of mass, angular velocity, and waveform of a thin-shell gravastar with $h_0 = 10^{-4}$, $M\Omega_0 = 0.25$, and $\tau/M = 0.041$ during the linear perturbation phase. The mass difference is rescaled by a factor 10 for better visualization.

$$\frac{\dot{M}}{M^3} = \alpha\beta\Omega\dot{\Omega}. \tag{4.9}$$

Integration of Eq. (4.9) yields

$$\Omega^2 = \Omega_0^2 + \frac{M_0^{-2} - M^{-2}}{\alpha\beta}. \tag{4.10}$$

The mass and the angular velocity can be obtained by solving the previous equations with the condition $dE/dt = -dM/dt$. A typical solution is shown in Fig. 8.

V. DISCUSSION

The above results show that ultracompact objects with high redshift at their surface are unstable when rapidly spinning. This strengthens the role of BHs as candidates for astrophysical observations of rapidly spinning compact objects.

Boson stars and gravastars easily develop ergoregion instabilities. Analytical and numerical results indicate that these objects are unstable against scalar field perturbations. Their instability time scale is many orders of magnitude stronger than the instability time scale for ordinary stars with uniform density [52]. In the large $l = m$ approximation, suitable for a WKB treatment, gravitational and scalar perturbations have similar instability time scales. In the low-m regime gravitational perturbations are expected to have shorter instability time scales than scalar perturbations.

For $J > 0.4M^2$ instability time scales can be as low as a few tenths of a second for solar-mass objects and about a week for supermassive BHs, monotonically decreasing for larger rotations. Therefore, high rotation is an indirect evidence for horizons. The spin of an astrophysical compact object can be estimated by looking at the gas accreting near its surface [2,70,71]. A handful of fast-spinning BH-like objects have been reported [6,7]. The results of this paper suggest that these objects must indeed be BHs.

The ergoregion instability evolution is characterized by very distinct waveforms. If compact astrophysical objects evolve through the ergoregion instability, gravitational-wave detectors could easily identify them with a matched-filtering search.

It would be interesting to repeat the above analysis for other ultracompact objects, such as wormholes [72–75], superspinars [76], and quark or fermion-boson stars [77]. The general arguments presented above suggest that these objects should be unstable. It would also be interesting to perform a more detailed analysis of the gravitational sector of the ergoregion instability and derive more refined templates for matched-filtering searches. A first step in this direction would be to compute axial perturbations for any value of the azimuthal number m along the lines of previous works [61].

ACKNOWLEDGMENTS

The authors are indebted to Emanuele Berti for many useful comments and suggestions, a critical reading of the manuscript, and for sharing some of his numerical routines with us. The authors warmly thank Burkhard Kleihaus, Jutta Kunz, and Isabell Schaffer for sharing and explaining their results concerning rotating boson stars. They also thank Óscar Dias and Kostas Kokkotas for interesting discussions and fruitful comments. This work was partially funded by Fundação para a Ciência e Tecnologia (FCT)—Portugal through Projects No. PTDC/FIS/64175/2006 and No. POCI/FP/81915/2007. M. C. gratefully acknowledges the support of the National Science Foundation through LIGO Research Support Grant No. NSF PHY-0757937.

[1] S. W. Hawking, Commun. Math. Phys. **25**, 152 (1972).
[2] R. Narayan, New J. Phys. **7**, 199 (2005).
[3] R. D. Blandford and R. L. Znajek, Mon. Not. R. Astron. Soc. **179**, 433 (1977).
[4] C. F. Gammie, S. L. Shapiro, and J. C. McKinney, Astrophys. J. **602**, 312 (2004).
[5] D. Merritt and M. Milosavljevic, Living Rev. Relativity **8**, 8 (2005).
[6] J. E. McClintock, R. Shafee, R. Narayan, R. A. Remillard, S. W. Davis, and L. X. Li, Astrophys. J. **652**, 518 (2006).
[7] J. M. Wang, Y. M. Chen, L. C. Ho, and R. J. McLure, Astrophys. J. **642**, L111 (2006).
[8] M. A. Abramowicz, W. Kluzniak, and J. P. Lasota, Astron. Astrophys. **396**, L31 (2002).
[9] J. P. Lasota, C.R. Physique **8**, 45 (2007).
[10] G. Chapline, E. Hohlfeld, R. B. Laughlin, and D. I. Santiago, Int. J. Mod. Phys. A **18**, 3587 (2003).
[11] P. O. Mazur and E. Mottola, arXiv:gr-qc/0109035.
[12] M. Visser and D. L. Wiltshire, Classical Quantum Gravity **21**, 1135 (2004).
[13] C. B. M. Chirenti and L. Rezzolla, Classical Quantum Gravity **24**, 4191 (2007).
[14] D. Horvat and S. Ilijic, Classical Quantum Gravity **24**, 5637 (2007).
[15] N. Bilic, G. B. Tupper, and R. D. Viollier, J. Cosmol. Astropart. Phys. 02 (2006) 013.
[16] F. S. N. Lobo, Classical Quantum Gravity **23**, 1525 (2006).
[17] F. S. N. Lobo and A. V. B. Arellano, Classical Quantum Gravity **24**, 1069 (2007).

[18] C. Cattoen, T. Faber, and M. Visser, Classical Quantum Gravity **22**, 4189 (2005). See also C. Cattoen, arXiv:gr-qc/0606011.
[19] D. J. Kaup, Phys. Rev. **172**, 1331 (1968); R. Ruffini and S. Bonazzola, Phys. Rev. **187**, 1767 (1969).
[20] V. Silveira and C. M. G. de Sousa, Phys. Rev. D **52**, 5724 (1995); S. Yoshida and Y. Eriguchi, Phys. Rev. D **55**, 1994 (1997); **56**, 762 (1997); **56**, 6370 (1997); F. E. Schunck and E. W. Mielke, Phys. Lett. A **249**, 389 (1998).
[21] F. E. Schunck and E. W. Mielke, Classical Quantum Gravity **20**, R301 (2003).
[22] E. Berti and V. Cardoso, Int. J. Mod. Phys. D **15**, 2209 (2006).
[23] M. Colpi, S. L. Shapiro, and I. Wasserman, Phys. Rev. Lett. **57**, 2485 (1986).
[24] T. D. Lee and Y. Pang, Phys. Rep. **221**, 251 (1992).
[25] D. F. Torres, S. Capozziello, and G. Lambiase, Phys. Rev. D **62**, 104012 (2000).
[26] F. S. Guzman, Phys. Rev. D **73**, 021501 (2006).
[27] M. Kesden, J. Gair, and M. Kamionkowski, Phys. Rev. D **71**, 044015 (2005).
[28] A. C. Fabian and C. R. Canizares, Nature (London) **333**, 829 (1988).
[29] R. Narayan, I. Yi, and R. Mahadevan, Nature (London) **374**, 623 (1995).
[30] A. E. Broderick and R. Narayan, Classical Quantum Gravity **24**, 659 (2007).
[31] W. H. G. Lewin, J. van Paradijs, and R. E. Taam, Space Sci. Rev. **62**, 223 (1993).
[32] B. F. Schutz, Classical Quantum Gravity **16**, A131 (1999); S. A. Hughes, Ann. Phys. (N.Y.) **303**, 142 (2003); L. P. Grishchuk, V. M. Lipunov, K. A. Postnov, M. E. Prokhorov, and B. S. Sathyaprakash, Usp. Fiz. Nauk **171**, 3 (2001); C. Cutler and K. S. Thorne, arXiv:gr-qc/0204090.
[33] http://www.ligo.caltech.edu/.
[34] http://www.cascina.virgo.infn.it/.
[35] http://tamago.mtk.nao.ac.jp/.
[36] http://lisa.nasa.gov/.
[37] E. Berti, A. Buonanno, and C. M. Will, Phys. Rev. D **71**, 084025 (2005); Classical Quantum Gravity **22**, S943 (2005); R. N. Lang and S. A. Hughes, Phys. Rev. D **74**, 122001 (2006); **75**, 089902(E) (2007).
[38] F. D. Ryan, Phys. Rev. D **52**, 5707 (1995); **56**, 1845 (1997).
[39] L. Barack and C. Cutler, Phys. Rev. D **75**, 042003 (2007).
[40] P. Amaro-Seoane, J. R. Gair, M. Freitag, M. Coleman Miller, I. Mandel, C. J. Cutler, and S. Babak, Classical Quantum Gravity **24**, R113 (2007).
[41] M. Vallisneri, Phys. Rev. Lett. **84**, 3519 (2000).
[42] C. Palenzuela, L. Lehner, and S. L. Liebling, Phys. Rev. D **77**, 044036 (2008).
[43] E. Berti, V. Cardoso, and C. M. Will, Phys. Rev. D **73**, 064030 (2006); E. Berti, V. Cardoso, J. A. Gonzalez, U. Sperhake, M. Hannam, S. Husa, and B. Bruegmann, Phys. Rev. D **76**, 064034 (2007); E. Berti, J. Cardoso, V. Cardoso, and M. Cavaglià, Phys. Rev. D **76**, 104044 (2007).
[44] S. Yoshida, Y. Eriguchi, and T. Futamase, Phys. Rev. D **50**, 6235 (1994); J. Balakrishna, R. Bondarescu, G. Daues, F. Siddhartha Guzman, and E. Seidel, Classical Quantum Gravity **23**, 2631 (2006).
[45] Ya. B. Zel'dovich, Pis'ma Zh. Eksp. Teor. Fiz. **14**, 270 (1971) [JETP Lett. **14**, 180 (1971)]; Zh. Eksp. Teor. Fiz. **62**, 2076 (1972) [Sov. Phys. JETP **35**, 1085 (1972)].
[46] A. A. Starobinsky, Zh. Eksp. Teor. Fiz. **64**, 48 (1973) [Sov. Phys. JETP **37**, 28 (1973)]; A. A. Starobinsky and S. M. Churilov, Zh. Eksp. Teor. Fiz. **65**, 3 (1973) [Sov. Phys. JETP **38**, 1 (1973)].
[47] J. D. Bekenstein and M. Schiffer, Phys. Rev. D **58**, 064014 (1998).
[48] W. H. Press and S. A. Teukolsky, Nature (London) **238**, 211 (1972).
[49] V. Cardoso, O. J. C. Dias, J. P. S. Lemos, and S. Yoshida, Phys. Rev. D **70**, 044039 (2004); **70**, 049903(E) (2004); V. Cardoso and O. J. C. Dias, Phys. Rev. D **70**, 084011 (2004); E. Berti, V. Cardoso, and J. P. S. Lemos, Phys. Rev. D **70**, 124006 (2004).
[50] J. L. Friedman, Commun. Math. Phys. **63**, 243 (1978).
[51] A. Vilenkin, Phys. Lett. **78B**, 301 (1978).
[52] N. Comins and B. F. Schutz, Proc. R. Soc. A **364**, 211 (1978).
[53] S. Yoshida and E. Eriguchi, Mon. Not. R. Astron. Soc. **282**, 580 (1996).
[54] J. B. Hartle, Astrophys. J. **150**, 1005 (1967); J. B. Hartle and K. S. Thorne, Astrophys. J. **153**, 807 (1968).
[55] B. F. Schutz and N. Comins, Mon. Not. R. Astron. Soc. **182**, 69 (1978).
[56] B. Kleihaus, J. Kunz, and M. List, Phys. Rev. D **72**, 064002 (2005); B. Kleihaus, J. Kunz, M. List, and I. Schaffer (unpublished).
[57] E. M. Butterworth and J. R. Ipser, Astrophys. J. **204**, 200 (1976).
[58] N. Stergioulas, Living Rev. Relativity **6**, 3 (2003).
[59] E. Berti, F. White, A. Maniopoulou, and M. Bruni, Mon. Not. R. Astron. Soc. **358**, 923 (2005).
[60] F. E. Schunck and E. W. Mielke, in *Relativity and Scientific Computing*, edited by F. W. Hehl, R. A. Puntigam, and H. Ruder (Springer, Berlin, 1996), p. 138.
[61] K. D. Kokkotas, J. Ruoff, and N. Andersson, Phys. Rev. D **70**, 043003 (2004).
[62] J. Ruoff and K. D. Kokkotas, Mon. Not. R. Astron. Soc. **330**, 1027 (2002).
[63] Y. Kojima, Phys. Rev. D **46**, 4289 (1992).
[64] V. Cardoso, O. J. C. Dias, J. L. Hovdebo, and R. C. Myers, Phys. Rev. D **73**, 064031 (2006).
[65] B. J. Owen, L. Lindblom, C. Cutler, B. F. Schutz, A. Vecchio, and N. Andersson, Phys. Rev. D **58**, 084020 (1998).
[66] P. Arras, E. E. Flanagan, S. M. Morsink, A. K. Schenk, S. A. Teukolsky, and I. Wasserman, Astrophys. J. **591**, 1129 (2003).
[67] E. E. Flanagan and S. A. Hughes, Phys. Rev. D **57**, 4535 (1998).
[68] B. J. Owen and L. Lindblom, Classical Quantum Gravity **19**, 1247 (2002).
[69] S. A. Teukolsky, Phys. Rev. Lett. **29**, 1114 (1972); Astrophys. J. **185**, 635 (1973).
[70] J. E. McClintock and R. A. Remillard, *Compact Stellar X-ray Sources*, edited by W. H. G. Lewin and M. van der Klis

(Cambridge University Press, Cambridge, England, 2004), Chap. IV.
[71] A. C. Fabian and G. Miniutti, arXiv:astro-ph/0507409.
[72] M. S. Morris and K. S. Thorne, Am. J. Phys. **56**, 395 (1988).
[73] M. Visser, *Lorentzian Wormholes: From Einstein to Hawking* (American Institute of Physics, NY, 1995).
[74] J. P. S. Lemos, F. S. N. Lobo, and S. Quinet de Oliveira, Phys. Rev. D **68**, 064004 (2003).
[75] T. Damour and S. N. Solodukhin, Phys. Rev. D **76**, 024016 (2007).
[76] E. G. Gimon and P. Horava, arXiv:0706.2873.
[77] A. B. Henriques, A. R. Liddle, and R. G. Moorhouse, Nucl. Phys. **B337**, 737 (1990); Phys. Lett. B **251**, 511 (1990); C. M. G. de Sousa and V. Silveira, Int. J. Mod. Phys. D **10**, 881 (2001); C. M. G. de Sousa and J. L. Tomazelli, Phys. Rev. D **58**, 123003 (1998); G. Narain, J. Schaffner-Bielich, and I. N. Mishustin, Phys. Rev. D **74**, 063003 (2006).